Giant magnetic anisotropy in doped single layer molybdenum disulfide and fluorographene

2016 J. Phys.: Condens. Matter 28 195301

(http://iopscience.iop.org/0953-8984/28/19/195301)

IOP Publishing Journal of Physics: Condensed Matter
J. Phys.: Condens. Matter **28** (2016) 195301 (6pp) doi:10.1088/0953-8984/28/19/195301

Giant magnetic anisotropy in doped single layer molybdenum disulfide and fluorographene

J Sivek, H Sahin, B Partoens and F M Peeters

Departement Fysica, Universiteit Antwerpen, Groenenborgerlaan 171, B-2020 Antwerpen, Belgium

E-mail: bart.partoens@uantwerpen.be

Received 24 December 2015, revised 9 March 2016
Accepted for publication 21 March 2016
Published 13 April 2016

Abstract

Stable monolayer materials based on existing, well known and stable two-dimensional crystal fluorographene and molybdenum disulfide are predicted to exhibit a huge magnetocrystalline anisotropy when functionalized with adsorbed transition metal atoms at vacant sides. *Ab initio* calculations within the density-functional theory formalism were performed to investigate the adsorption of the transitional metals in a single S (or F) vacancy of monolayer molybdenum disulfide (or fluorographene). We found strong bonding of the transitional metal atoms to the vacant sites with binding energies ranging from 2.5 to 5.2 eV. Our calculations revealed that these systems with adsorbed metal atoms exhibit a magnetic anisotropy, specifically the structures including Os and Ir show a giant magnetocrystalline anisotropy energy of 31–101 meV. Our results demonstrate the possibility of obtaining stable monolayer materials with huge magnetocrystalline anisotropy based on preexisting, well known and stable two-dimensional crystals: fluorographene and molybdenum disulfide. We believe that the results obtained here are useful not only for deeper understanding of the origin of magnetocrystalline anisotropy but also for the design of monolayer optoelectronic devices with novel functionalities.

Keywords: magnetic anisotropy, molybdenum disulfide, fluorographene

(Some figures may appear in colour only in the online journal)

1. Introduction

Graphene [1, 2] and similar two-dimensional materials such as semiconductor transition metal dichalcogenides (sTMDs) [3, 4] have gained increasing attention over the past 10 years. Most of the unique properties and possible novel functionalities of these ultra-thin structures originate from quantum confinement effects and their exceptional crystal symmetry. In addition, controllable doping provides a directed and effective approach to elevate or induce specific characteristics in these two-dimensional crystals [5]. One such material property is magnetic anisotropy. Materials with a high magnetocrystalline anisotropy [6] are of interest for magnetoelectronics technology to manufacture data storage components [7], as well as for spintronics applications where increased anisotropy is used to realize a high degree of spin polarization [8]. The search for nanostructures with high magnetic anisotropy is also fueled by the need to reduce the size of ferromagnetic components, e.g. for long-term magnetic data storage.

In the past it was demonstrated that magnetic anisotropy can be induced by chemical functionalization of pristine materials, e.g. in graphene decorated with transition metal atoms the strong hybridization between adatoms and the graphene C atoms induce magnetic anisotropy [9–12], in MoS_2 crystals the magnetic anysotropy can be controlled by hydrogenation and proton irradiation [13], and this is valid especially for ultrathin materials [14]. Especially adsorbates with 4*d* and 5*d* transition metals (TM) have shown promising results for the realisation of large uniaxial magnetic anisotropies with magnetocrystalline anisotropy energy (MAE) values of the order of several 10 meV [12, 15], or even up to the 100 meV for transition metal dimers on graphitic surfaces [12, 16].

Such large MAE values are of high interest because they allow for applications with a long retention time for magnetization at high temperatures.

Here we investigate monolayer structures of fluorographene (FG) and molybdenum disulfide (MoS_2) as a chemically and structurally stable basis for the chemical functionalization by TM atoms in order to induce a large magnetic anisotropy. We present the structural stability, magnetic properties and MAEs of single layer S-vacant MoS_2 and F-vacant FG decorated with W, Os, Ir, Pt, Ru, Rh or Co atoms located at the vacancies. Very recently, we have also investigated the magnetic anisotropy characteristics of novel monolayer two-dimensional materials such as $FeCl_2$, graphone and $MoTe_2$ [17].

2. Computational methodology

All geometry optimizations and electronic structure calculations were carried out by means of the VASP package [18] and with the use of spin polarized Perdew, Burke, and Ernzerhof [19] (PBE) generalized gradient (GGA) parametrization for the exchange-correlation functional. We made use of the projector augmented wave method [20] and a plane-wave basis set with an energy cutoff of 500 eV. The sampling of the Brillouin zone was done for the supercell with the equivalent of a $24 \times 24 \times 1$ Monkhorst–Pack k-point grid for both the FG and MoS_2 primitive unit cell. The partial occupancies in the electronic ground state calculation were treated using the tetrahedron methodology with Blöchl corrections [21]. The reported quantitative results of the charge transfers were obtained using the Bader charge population analysis [22, 23]. MAE values were calculated by employing a direct, two step process. First, a Kohn–Sham based calculation with collinear electron density and without spin–orbit coupling corrections was performed in order to obtain a self-consistent ground state electronic charge density. In the second step, the obtained charge density was used as an input for the non self-consistent spin–orbit coupling and non-collinear calculations with varying orientation of the magnetic moments.

The fundamentals of the employed *ab initio* methodology allows one to obtain a self-consistent relativistic potential directly from the pseudo-wavefunctions following the construction methods in the studies of Hamann *et al* [24] Kleinman [25] and Błoński *et al* [26] The spin–orbit interaction is evaluated in the Hamiltonian with the following contribution from each atom in the supercell (with only spherical dependence on the potential within the restricted region) [27]:

$$H^{\mathrm{so}} = \frac{1}{2(m_{\mathrm{e}}c)^2}\frac{1}{r}\frac{\mathrm{d}V}{\mathrm{d}r}\vec{L}\cdot\vec{S} \qquad (1)$$

with m_{e} the electron mass, r the radial distance from individual atom nuclei, V the potential around the nuclei, $\vec{L}$ and $\vec{S}$ the orbital momentum and spin operators. The spin–orbit interactions lead to the nonzero MAE for the adatom-monolayer crystal structures, considered in this study, when varying direction of the magnetic moments. As long as the spin–orbit coupling is ignored rotation of all the magnetic moments in the system by the same angle results in the same total energy.

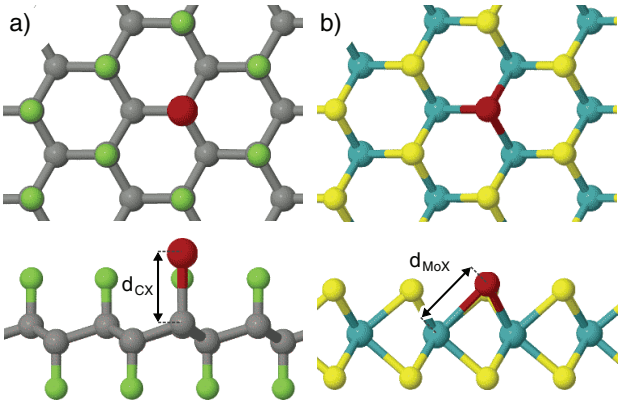

Figure 1. Top and side view of the relaxed structures of (a) fluorographene and (b) molybdenum disulfide. C, F, Mo, S and adatoms are depicted with gray, green (light), green (dark), yellow (light) and red (murky) colors, respectively. The carbon–transition metal distance d_{CX} and the molybdenum–transition metal distance d_{MoX} are displayed as well.

The magnetocrystalline anisotropy energy is computed as the energy difference between in plane magnetization ($E_{\parallel}$) and perpendicular magnetization ($E_{\perp}$) which is given by the formula:

$$\mathrm{MAE} = E_{\parallel} - E_{\perp}. \qquad (2)$$

The positive (negative) value of the MAE implies that the easy magnetization axis is perpendicular (parallel) to the surface of the two-dimensional crystal. The diagonal x–y axis was selected as in-plane magnetization axis. The effect of in-plane rotation of the magnetization axis is discussed later. Presence of such an anisotropic behavior in a crystal structure stems from the interaction of the spins with the field generated by the electron orbital motion and it is fundamentally a relativistic effect.

3. Structural properties and stability

The systems under study are composed of a 3×3 supercell of FG and MoS_2 with a single F or S atom vacancy, respectively, in which a transition metal atom is adsorbed. This is equivalent to ∼5.5% coverage of TM atoms per C and/or Mo atom. The structure and placement of the adsorbed atom are indicated in figure 1. The structural properties including the lattice parameter as well as the TM atom to C (or Mo) atom distance are reported in table 1. The adsorption of the metal atom on the vacant site of the MoS_2 does not result in a significant lattice distortion. Compared to the pristine MoS_2 lattice parameter 9.56 Å (for a 3×3 supercell) the adsorption induces a moderate decrease by as much as ∼0.5%, with one exception for the Os atom, where the lattice parameter is enlarged by ∼0.1%. A similar decrease of lattice constant, by as much as ∼0.6%, is found for doped FG with a pristine lattice parameter of 7.84 Å (for a 3×3 supercell).

In order to address the stability of the predicted structures we evaluate the binding energy. It is defined as $E_{\mathrm{b}} = (E_{\mathrm{vacant}} + E_{\mathrm{TM}}) - E_{\mathrm{system}}$, with E_{system} the total energy of

Table 1. Electronic, magnetic and structural properties of a transition metal adatom bonded to single layer MoS_2 and fluorographene.

	a (Å)	d (Å)	E_b (eV)	μ (μ_B)	ρ (e)	p e · (Å)	MAE (meV)
Pt-FG	7.81	2.03	2.71	1	0.36	0.43	5.46
Rh-FG	7.79	2.11	3.14	2	0.56	0.55	7.77
Ru-FG	7.79	2.13	2.84	3	0.66	0.56	−11.24
Co-FG	7.79	1.98	3.01	2	0.67	0.58	1.24
Ir-FG	7.81	2.05	2.72	2	0.44	0.42	52.79
Os-FG	7.80	2.08	2.45	3	0.54	0.40	−100.46
W-FG	7.80	2.25	2.58	5	0.73	0.39	−47.02
Pt-MoS_2	9.54	2.63	5.24	0	−0.38	0.16	0.00
Rh-MoS_2	9.53	2.62	4.66	1	−0.12	0.19	−3.21
Ru-MoS_2	9.53	2.62	4.58	2	0.06	0.23	9.92
Co-MoS_2	9.51	2.49	3.78	1	0.12	0.19	2.24
Ir-MoS_2	9.54	2.52	5.15	1	−0.31	0.16	31.14
Os-MoS_2	9.58	2.57	4.88	2	−0.11	0.22	36.30
W-MoS_2	9.54	2.60	4.62	2	0.44	0.32	−40.65

Note: These atoms are attached at the position of a missing sulfur or fluorine atom, respectively. The table provides the following parameters: the lattice constant (a), substitute–carbon (or molybdenum) distance (d), binding energy per TM atom (E_b), magnetic moment per TM atom (μ), charge located on the adatom (ρ), dipole moment per TM atom (p) and magnetocrystalline anisotropy energy (MAE) per TM atom.

the system with adsorbed TM atom, E_{vacant} the total energy of the system with the vacancy, and E_{TM} the energy of a single TM atom, all in the corresponding supercell. All the TM decorated systems are stable as can be seen from the considerable positive values of the binding energies, in table 1, ranging from 3.78 to 5.24 eV per adatom for doped MoS_2 and 2.45 to 3.14 eV per adatom for doped FG. The binding of TM atoms to MoS_2 is up to 2.5 eV larger compared to FG, this is especially prominent for Pt, Ir and Os adatoms. Consistent with the electronegativity of the elements, with the C atom carrying the highest value, all the TM atoms are positively charged and donate electrons mainly to the bonded C atom when adsorbed on F-vacant FG. On the other hand Pt, Ir and partially Os adatoms behave like acceptors on S-vacant MoS_2.

MoS_2 as well as FG are materials composed of three atomic layers. Due to the difference in the electronegativity the outer layers composed of F atoms or S atoms are charged negatively while leaving the middle layer composed of positively charged C atoms or Mo atoms. Addition of the TM adatom, which has a smaller electronegativity compared to both F or S atoms, into the single vacancy creates locally a decrease of the electron density, reducing the amount of surplus of the negative charge in the upper layer compared to the bottom layer. This change induces a dipole moment pointing from the pristine to the adsorbed side of 0.39 to 0.58 e · Å for FG and 0.16 to 0.32 e · Å for MoS_2.

4. Inducing MAE in fluorographene

The calculated MAE values of the chemically decorated F vacant FG are given in table 1. The Os, Ir and W atoms induce a strong magnetocrystalline anisotropy with MAE values

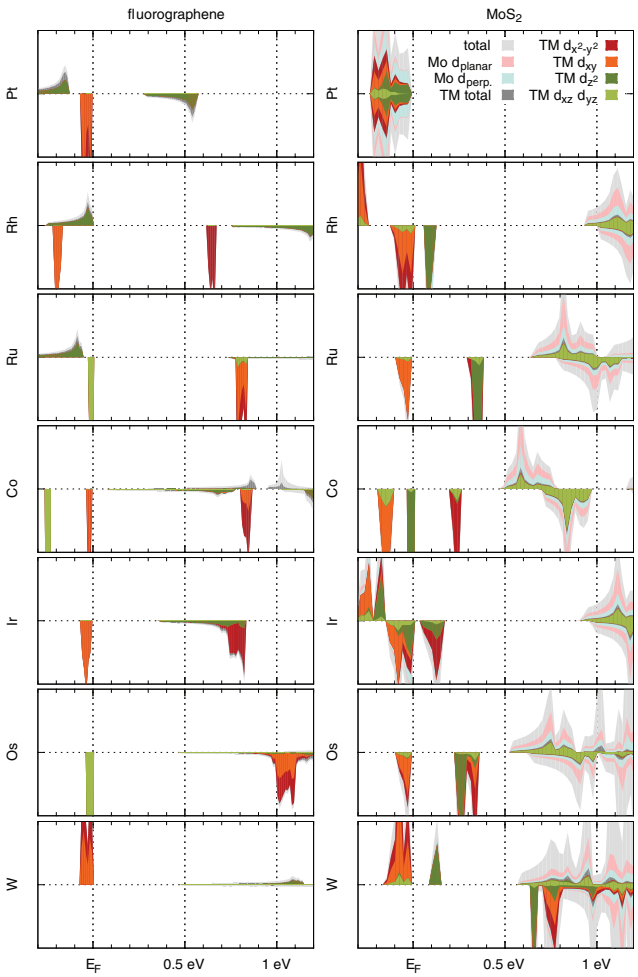

Figure 2. Orbital projected density of states for TM atom decorated FG and MoS_2. The total density of states includes only adatoms and bonded atoms from the substrate (three neighboring Mo atoms in MoS_2 and four C atoms in FG, first and second nearest neighbor). The majority of the pictured mid-gap states do have origin in TM adatoms and their orbital character is denoted in the legend with labels starting with the 'TM' prefix. The Fermi energy is set to 0 eV.

of −100.46 meV, 52.79 meV and −47.02 meV, respectively. With exception of Os, W and Ru adatoms, the orientation of the easy axis corresponds to the perpendicular direction.

We observe that an essential requirement to realize a non zero MAE is the presence of a net magnetic moment. In general we deduce from the results in table 1 that a higher magnetization of the ground state leads to higher MAE values (although there are exceptions, see for example for the W adatom on FG). Furthermore, the magnetic anisotropy depends on the spin–orbit coupling of the adatoms. This characteristic is dominant for a Pt atom which induces a higher MAE of 5.46 meV, compared to 1.24 meV for a Co atom, despite its lower magnetic moment.

To obtain further insight into the origin of the magnetocrystalline anisotropy we show the calculated orbital projected density of states in figure 2. Adsorption of a TM atom on FG results in a spin-polarized ground state. Unlike free atoms, with all the d orbitals at the same energy level, the C atoms surrounding the adatom lead to a crystal field splitting of the d orbitals of the TM adatom. The resulting d level

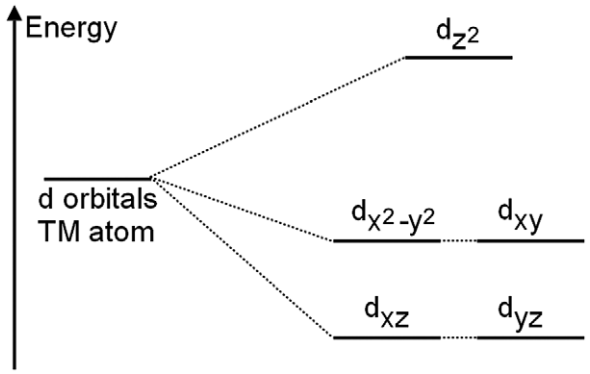

Figure 3. Schematic picture of the observed trigonal crystal field splitting of the *d* levels of the adsorbed TM atom.

splitting based on the position of the projected orbitals of the minority spins is shown in figure 3. It corresponds to a trigonal level splitting, in agreement with the local trigonal symmetry around the adatom. The deviation from the known planar trigonal level splitting is only in the position of the d_{z^2} orbital: due to the buckling it is the orbital with the highest energy, while in the planar trigonal case it is the central orbital (note that in the case of W, the order is indeed switched with $d_{x^2-y^2}$ and d_{xy} the highest levels). The spin-polarized ground state also explains why the magnetic moment gradually decreases with increase of the TM atomic number in the corresponding row of the periodic table of elements (see table 1). Vacant FG itself possesses a magnetic moment of 1 μ_B, one per F vacancy, originating from the dangling bond of the sp^3 hybridized C atom. The TM adatoms have one *s* and five *d* valence orbitals. The TM adatom creates a bond with this underlying C atom, leaving five orbitals to be occupied with the resulting valence electrons of the TM adatom (i.e. the number of valence electrons of the free TM adatom minus one). This explains why the resulting magnetic moments in table 1 equal $5 - [(\text{number of valence electrons of the TM adatom}) - 1 - 5]$.

While magnetization of adatom decorated FG could be manipulated by an external magnetic field in different directions, the stability of a specific magnetization direction is determined by the TM atom bonding coordination, the geometry, as well as by the occupation of the electronic states close to the Fermi level. We can indeed make a link between the geometrical character of the valence states close to the Fermi level dtermined by the crystal field splitting and the easy axis orientation. The Os adatom induces a giant negative MAE with a value of −100.46 meV and shows perpendicularly oriented d_{xz} and d_{yz} highest occupied molecular orbital (HOMO) states (lower left panel in figure 2). On the other hand Pt, Ir and Co adatoms induce a perpendicular easy axis, and create valence states dominated by planar d_{xy} and $d_{x^2-y^2}$ states. It can be expected that planar motion will lead to a dominant orbital magnetic moment perpendicular to this plane, while motion in the perpendicularly oriented HOMO states will lead to a dominant orbital moment within this plane. Thus in these cases the orientation of the easy axis corresponds to the direction of the dominant orbital magnetic moment near the Fermi level, very similar to the consequences of the the Bruno model for magnetocrystalline anisotropy [14]. The same trend

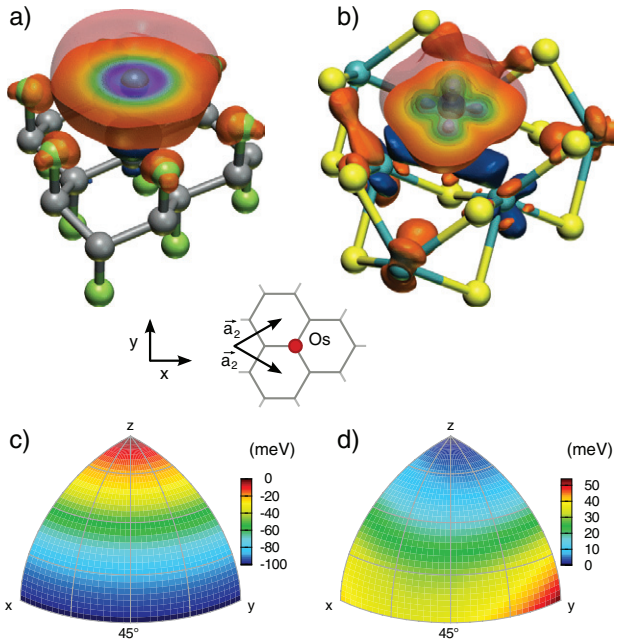

Figure 4. (a), (b) The magnetization charge densities are displayed for Os adsorbed fluorographene and MoS_2, respectively (the isosurface is set to 10^{-2} e Å^{-3} for majority, orange (bright), and minority, blue (dark), spin charge densities). Lower, in insets (c) and (d) the variations of MAE values are projected on the sphere for Os adsorbed fluorographene and MoS_2, respectively. The displayed values are computed as: $\text{MAE} = E_{\text{axis}} - E_{\perp}$, with E_{axis} the magnetization energy with the magnetization axis corresponding to the point on the sphere.

is observable for Ru and partially for Rh adatoms, the observations are of opposite nature for W decorated FG. Moreover, the splitting of HOMO and lowest unoccupied molecular orbital (LUMO) energy bands of Pt, Ir and Os decorated FG correlates with the absolute value of the MAE.

5. Inducing MAE in MoS_2

The calculated MAE values of the chemically decorated vacant MoS_2 are given in table 1. Although the induced MAE values are lower compared to FG, we observe a strong induced magnetocrystalline anisotropy for adsorbed W, Os and Ir atoms with MAE values of −40.65 meV, 36.3 meV and 31.14 meV, respectively. All, but W and Rh, adatoms induce a perpendicular easy axis.

The origin of the magnetic moment in doped MoS_2 is of a more complex nature than in doped FG and can have a mixture of causes. The magnetic states in decorated S vacant MoS_2 are more spread compared to FG as they extend up to the nearest Mo neighbour atoms for Co and Ir adsorption and even the next nearest Mo neighbour atoms for Os adsorption (compare the magnetization charge density for the example of Os or Ir adatom on MoS_2 and FG in figures 4(a) and (b) or figures 5(a) and (b)). Nevertheless, the total magnetic moment can be obtained in a similar way as for the FG case. As S has one less valence electron than F, the removal of an S atom leaves two electrons behind in the vacancy. The adatom will form a bond with these electrons, leaving only four orbitals to be filled with the

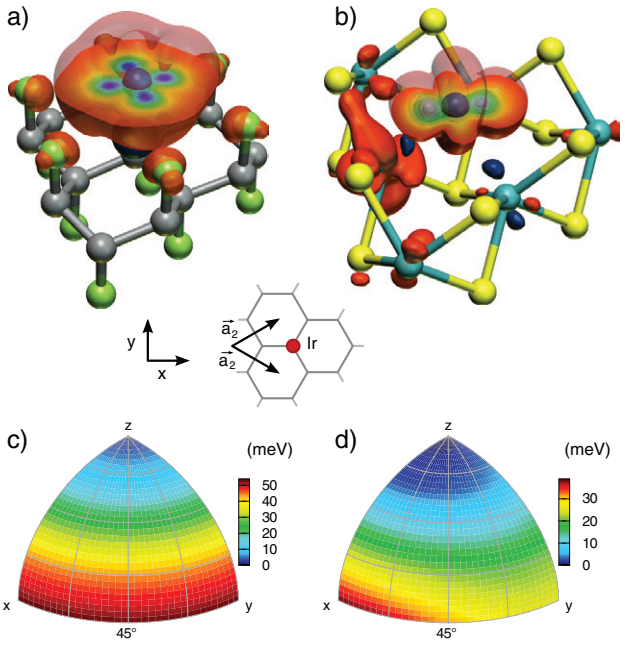

Figure 5. (a), (b) The magnetization charge densities are displayed for Ir adsorbed fluorographene and MoS_2, respectively (the isosurface is set to 10^{-2} e Å^{-3} for majority, orange (bright), and minority, blue (dark), spin charge densities). Lower, in insets (c) and (d) the variations of MAE values are projected on a sphere for Ir adsorbed fluorographene and MoS_2, respectively. The displayed values are computed as $\mathrm{MAE} = E_{\mathrm{axis}} - E_{\perp}$, with E_{axis} the magnetization energy with the magnetization axis corresponding to the point on the sphere.

remaining valence electrons of the adatom. Together with the high spin configuration, this leads to the magnetic moments of $4 -$ [(Number of valence electrons of the TM adatom) $- 2 - 4$] in table 1. (The only exception is W decorated MoS_2, which is not in the high spin configuration. Figure 2 shows that the d_{z^2} orbital is empty, leading to a magnetic moment of 2 μ_B.)

Unlike in decorated FG the TM adatoms on MoS_2 exhibit three coordination bonding to the neighbouring Mo atoms. As can be seen in figure 4(b) and in figure 5(b), the magnetization charge density induced by the TM atom adsorbed on MoS_2 is not axially symmetric and its symmetry does not correspond to the three fold symmetry implied by the bonding, compared to figure 4(a). This discrepancy in the symmetries induces slightly asymmetric bonds. Nevertheless, the same crystal field splitting of figure 3 is observed in the orbital projected density of states, shown in the second column of figure 2.

It is also important to discuss the effect of this magnetization charge density symmetry on the calculated MAE values. Figures 4(c), (d) and 5(c), (d) show the MAE values for Os and Ir on FG and MoS_2, respectively, for arbitrary magnetization axes. The strong anisotropy of the magnetization charge density induced by TM atoms adsorbed on MoS_2 markedly induces a dependence of the MAE value on the orientation of the parallel magnetization axis. The effect is negligible for decorated FG.

The aforementioned observations of the relation between the magnetic moment, the orbital character of the HOMO levels and the magnetic anisotropy in FG can now be applied to doped MoS_2. The lower magnetic moments lead to lower values for the MAE (see table 1), up to the point of Pt decoration of MoS_2 with a rather strong binding energy (5.24 eV) and a nonmagnetic ground state leading to zero MAE (compared to 5.46 meV for Pt-FG). The MAE value for the Os adatom case, 36.30 meV, is larger than for the Ir adatom, 31.14 meV, thanks to a larger magnetic moment. Next, we can deduce the orientation of the easy axis. The Co, Ru, Ir as well as Os adatoms induce HOMO states predominantly composed out of planar d_{xy} and $d_{x^2-y^2}$ states. The geometrical character is translated into an easy axis perpendicular to the surface. The same trend cannot be deduced for adsorbed Rh and W atoms, however the W adatom shows a compatible behaviour for both the MoS_2 and FG substrate. In accordance with doped FG, the increased band gap in doped MoS_2 properly indicates the differences in the absolute size of MAE.

We observe mutually compatible trends for the magnetic anisotropy of doped MoS_2 and FG. Clues in the form of the net magnetic moment of the structure and the orbital character of the HOMO states determined by the crystal field splitting are found to be sufficient to provide a general insight into the calculated magnetocrystaline anisotropy. Nevertheless, it is important to note that the aforementioned recipe for large MAE values does not give a comprehensive explanation of the origin of the magnetic anisotropy. This is underlined by the fact that the observed general trend is of a different nature than the one described in the earlier works of Honolka *et al* [28]. The fundamental adatom properties like larger covalent radius, structure of the atomic shell that has a direct influence on the larger spin–orbit interaction, or the magnetic moment per adatom which enhances the calculated MAE values (for calculated magnetic moments up to the 3 μ_B per adatom the corresponding MAE values increase respectively with magnetic moment), are indispensable indicators of the magnetic anisotropy, yet they are just parts of the complex origin of this physical property.

Finally it is also important to note that the here presented computational results do not include on site Coulomb and exchange interactions. However, we have performed a limited set of calculations incorporating Hubbard corrections to the density functional theory (DFT) energy functional (also known as DFT + U) with an arbitrary U parameter. These calculations revealed that the inclusion of on site Coulomb and exchange interactions do not alter the easy axis direction. On the other hand DFT + U corrections can result in a decrease of the MAE values. For example, if we choose $U = 1$, the MAE value for Os decorated MoS_2 reduces from 36.30 meV to 20.29 meV, and for Os decorated FG from -100.46 meV to -80.57 meV. The reason why we provide only rough information about the DFT + U results stems from the nature of the studied systems. The proposed crystals are not yet realized experimentally and the amount of known material properties of molybdenum disulfide as well as fluorographene is limited, thus the U correction term cannot yet be determined experimentally. On the other hand, the *ab initio* calculation of an exact U parameter will increase the computational cost tremendously.

6. Conclusion

In summary, we performed an *ab initio* study of transition metal atom (W, Os, Ir, Pt, Ru, Rh and Co) adsorption in single F-vacant (S-vacant) FG (MoS_2). It was shown that transition metal atoms form stable structures when adsorbed in vacant sites on monolayer FG and MoS_2. We found giant magnetocrystalline anisotropy energy values for these low-dimensional crystal structures. The reduced symmetry, due to the asymmetric charge distribution at adatom adsorption sites, spin-polarized ground state of the compound and orbital character of the electronic band states around the Fermi level result in the observed magnetocrystalline anisotropy. The obtained results should provide a useful base for further study of the magnetocrystalline anisotropy and a motivation for the potential design of monolayer optoelectronic devices with novel functionalities.

This work was supported by the Flemish Science Foundation (FWO-Vl) and the Methusalem foundation of the Flemish Government. Computational resources were provided by TUBITAK ULAKBIM, High Performance and Grid Computing Center (TR-Grid e-Infrastructure), and HPC infrastructure of the University of Antwerp (CalcUA) a division of the Flemish Supercomputer Center (VSC), which is funded by the Hercules foundation. HS is supported by a FWO Pegasus-long Marie Curie Fellowship.

References

[1] Novoselov K S, Geim A K, Morozov S V, Jiang D, Zhang Y, Dubonos S V, Grigorieva I V and Firsov A A 2004 *Science* **306** 666
[2] Geim A K and Novoselov K S 2007 *Nat. Mater.* **6** 183
[3] Coleman J N *et al* 2011 *Science* **331** 568
[4] Ataca C, Şahin H and Ciraci S 2012 *J. Phys. Chem.* C **116** 8983
[5] Komsa H P, Kotakoski J, Kurasch S, Lehtinen O, Kaiser U and Krasheninnikov A V 2012 *Phys. Rev. Lett.* **109** 035503
[6] Šipr O, Bornemann S, Ebert H and Minár J 2014 *J. Phys.: Condens. Matter* **26** 196002
[7] Xiao R, Fritsch D, Kuz'min M D, Koepernik K, Eschrig H, Richter M, Vietze K and Seifert G 2009 *Phys. Rev. Lett.* **103** 187201
[8] Lukaszew R A, Sheng Y, Uher C and Clarke R 1999 *Appl. Phys. Lett.* **75** 1941
[9] Rougemaille N, N'Diaye A T, Coraux J, Vo-Van C, Fruchart O and Schmid A K 2012 *Appl. Phys. Lett.* **101** 142403
[10] Donati F, Dubout Q, Autès G, Patthey F, Calleja F, Gambardella P, Yazyev O V and Brune H 2013 *Phys. Rev. Lett.* **111** 236801
[11] Beljakov I, Meded V, Symalla F, Fink K, Shallcross S, Ruben M and Wenzel W 2014 *Nano Lett.* **14** 3364
[12] Hu J and Wu R 2014 *Nano Lett.* **14** 1853
[13] Han S W *et al* 2013 *Phys. Rev. Lett.* **110** 247201
[14] Bruno P 1989 *Phys. Rev.* B **39** 865
[15] Zhang H, Lazo C, Blügel S, Heinze S and Mokrousov Y 2012 *Phys. Rev. Lett.* **108** 056802
[16] Hao Z and Tchernyshyov O 2009 *Phys. Rev. Lett.* **103** 187203
[17] Torun E, Sahin H, Bacaksiz C, Senger R T and Peeters F M 2015 *Phys. Rev.* B **92** 104407
[18] Kresse G and Furthmüller J 1996 *Phys. Rev.* B **54** 11169
[19] Perdew J P, Burke K and Ernzerhof M 1996 *Phys. Rev. Lett.* **77** 3865
[20] Blöchl P E 1994 *Phys. Rev.* B **50** 17953
[21] Blöchl P E, Jepsen O and Andersen O K 1994 *Phys. Rev.* B **49** 16223
[22] Bader R F W 1991 *Chem. Rev.* **91** 893
[23] Henkelman G, Arnaldsson A and Jónsson H 2006 *Comput. Mater. Sci.* **36** 354
[24] Hamann D R, Schlüter M and Chiang C 1979 *Phys. Rev. Lett.* **43** 1494
[25] Kleinman L 1980 *Phys. Rev.* B **21** 2630
[26] Błoński P, Dennler S and Hafner J 2011 *J. Chem. Phys.* **134** 034107
[27] Min H, Hill J E, Sinitsyn N A, Sahu B R, Kleinman L and MacDonald A H 2006 *Phys. Rev.* B **74** 165310
[28] Honolka J *et al* 2012 *Phys. Rev. Lett.* **108** 256811